Advanced turbulence modeling improves thermal gradient prediction during compressed hydrogen tank filling

Rémi Gonin, Pierre Horgue, Romain Guibert, David Fabre, Rémi Bourguet, Fouad Ammouri, Elena Vyazmina

Advanced turbulence modeling improves thermal gradient prediction during compressed hydrogen tank filling

Rémi GONIN[a,b,*], Pierre HORGUE[a], Romain GUIBERT[a], David FABRE[a], Rémi BOURGUET[a], Fouad AMMOURI[b], Elena VYAZMINA[b]

[a] *Institut de mécanique des fluides de Toulouse (IMFT), Université de Toulouse, CNRS, 2 allée Camille Soula, Toulouse, France*
[b] *Air Liquide Innovation Campus Paris, 1 Chemin de la Porte des Loges, Les Loges-en-Josas, France*

Abstract

In order to use gaseous hydrogen for mobility of light and heavy duty vehicles, the standard J2601 from the Society of Automotive Engineers (SAE) recommends that the temperature in the tank must not exceed 85 $°C$ for safety reasons. Prior experiments reported that a vertical thermal stratification can occur during the filling of horizontal tanks under specific conditions. Thermodynamic modeling of hydrogen tank filling can predict the average gas temperature but not the onset of stratification. In a previous study, the computational fluid dynamics (CFD) software OpenFOAM was used to carry out simulations of hydrogen filling for a type IV 37 L tank. The CFD results, by comparison with experimental results from the HyTransfer project, were capable to predict the rise of the thermal stratification with however an underestimation of thermal gradient magnitudes. The maximal temperature predicted at the end of the filling was 15.05 $°C$ bellow the experimental measurements. In this work, the $k-\omega$ SST turbulence model is replaced by the $k-\omega$ SST SAS turbulence model to limit the prediction of high levels of eddy-viscosity in stagnation areas which over-diffuses the temperature. By using the same mesh as in a previous study, (651 482 cells in the fluid region and 449 126 cells in solid regions), the $k-\omega$ SST SAS turbulence model is found to be more appropriate for CFD simulation of tank filling as it predicts a thermal gradient magnitude in the gas in better agreement with experimental measurements than the $k-\omega$ SST turbulence model for a similar time of simulation. The maximal temperature predicted at the end of the filling is 2.17 $°C$ bellow the experimental measurements.

Keywords: high-pressure hydrogen, tank filling, thermal stratification, CFD, turbulence modeling

*Corresponding author
Email address: remi.gonin@airliquide.com (Rémi GONIN)

1. Introduction

The use of hydrogen as an energy carrier is motivated by its ability to produce electrical power without rejecting CO_2 to the atmosphere. The COP 26 summit urges on a net-zero target of greenhouse gas emissions for mid-century [1]. Hydrogen can replace fossil-fuel to match this requirement [2].

In this perspective, the automotive industry develops high pressure storage of hydrogen for light and heavy duty [3] fuel-cell vehicles. During the filling of gaseous tanks, the gas pressure is increasing and induces an elevation of the gas temperature. In the J2601 standard, the Society of Automobile Engineers (SAE) organism [4] recommends to maintain the maximum temperature inside the tank below 85 $°C$. Type IV tanks use plastic as liner and a composite material wrap around to limit tank weight and endure the pressure force of the 700 *bar* compressed hydrogen. These materials are thermal insulators, which limits heat exchanges between the compressed gas in the tank and the exterior environment. Type IV tanks are likely to exceed 85 $°C$ during filling.

The final averaged gas temperature in the tank depends on the temperature of the injected hydrogen [5, 6]. A cooling process is applied to the injected hydrogen to maintain the final averaged temperature below 85 $°C$. The final averaged gas temperature also depends on the filling time. A shorter filling time, which requires a higher mass flowrate, limits heat exchanges between the inner gas and the walls of the tank [7, 8]. However, for a longer filling time, i.e. a smaller mass flowrate, the injected gas has a lower velocity, limiting the mixing process inside fluid bulk. A criterion of 5 m/s for the velocity of the gas at the injection was suggested in [9] to maintain the mixing for a type IV 65 L tank with an aspect ratio of 2.08. This criterion was confirmed in subsequent studies [10, 11]. A limited mass flowrate may lead to thermal heterogeneities inside the tank: despite the fact that the averaged temperature is within the thermal recommendation, local hot spots exceeding the thermal recommendation can occur.

The HyTransfer project [12] investigated the filling of hydrogen tanks laid horizontally for different tank geometries and different filling scenarios. During the experiments, a type IV 37 L tank provided by ®Hexagon (with a length to diameter aspect ratio of 2.4) showed contrasted thermal behaviors, depending on the injection diameter and mass flowrate. Figure 1 shows a schematic of the tank and presents the fluid region and the different solid regions. The experimental measurements from Air Liquide Advanced Technology (ALAT) used 10 probes of temperature in the fluid region. Their locations are represented in figure 1.

These experimental measurements were performed for 3 injector diameters (3 mm, 6 mm and 10 mm) and 2 mass flowrates (2 g/s and 8 g/s). The 10 mm diameter is obtained by injecting directly through the plug aperture, without injection pipe. The above mentioned mass flowrate values are averaged over the filling time. To designate them, the injection diameter D and the mass flowrate Q followed by the corresponding values are used. For example, the case D10Q2 corresponds to the scenario with the injector diameter of 10 mm and the averaged mass flowrate of 2 g/s. Table 1 presents different filling scenarios

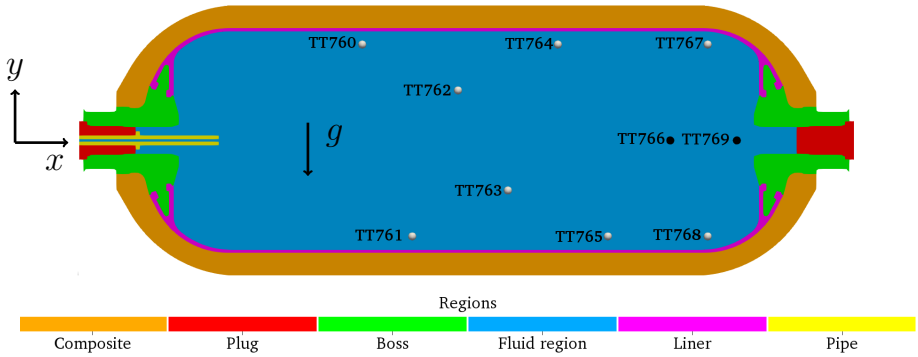

Figure 1: Type IV 37 L tank provided by ®Hexagon filled axially in horizontal position with a 3 mm diameter injector. View through the (x,y) plane. Probe locations are marked on the schematic by circles: probes located inside the (x,y) plane in white and probes located outside the (x,y) plane in black.

Scenario name	D3Q2	D3Q8	D6Q2	D6Q8	D10Q2	D10Q8
Injection diameter $[mm]$	3	3	6	6	10	10
Time-averaged mass flowrate $[g/s]$	2	8	2	8	2	8
Velocity at pipe outlet* [max; min]$[m/s]$	[190;4.2]	[280;17]	[62;1.1]	[73;2.0]	[22;0.41]	[28;1.1]
$T_{max} - T_{av}$ $[°C]$	8.36	6.35	26.76	11.28	30.03	24.39

Table 1: Thermal gradients for the type IV 37 L tank from ALAT[13]. *The velocity at pipe outlet is given in brackets to indicate the range of velocities during the filling. It is estimated assuming a uniform velocity profile in the pipe and using the density calculated via the measured inlet temperature and pressure in the tank, the measured mass flowrate and pipe cross section. As the density is rising during the filling and the mass flowrate does not vary too much, the velocity at pipe outlet is largely diminishing during the filling.

with the thermal gradient occurring at the end of the filling and an estimate of the injection velocity. To complement table 1, figure 2 gives the temperatures measured during the experimental campaigns [13] for the above mentioned cases.

Views (A) and (F) are the extreme scenarios in terms of thermal gradients: (A) is the most homogeneous case and (F) the most heterogeneous case. These two cases were studied previously [14] using three dimensional (3D) computational fluid dynamics (CFD) simulations performed with the software OpenFOAM[15]. The geometrical domain selected for the simulations was a half of the tank geometry, using a symmetry assumption about the (x,y) plane to save computational resources. The D3Q8 CFD results matched the experimental data regarding both the averaged temperature and the local probe temperatures in the fluid. The D10Q2 CFD results matched the experimental data regarding the averaged temperature of the fluid and detected the onset of stratification. However, the thermal stratification magnitude was underestimated. This is consistent with the results of ALAT [16] where the same turbulence model, the $k-\omega$ Shear Stress Transport (SST) model [17] was used, with a different CFD code and a different mesh.

Figure 3, issued from a previous study [14], summarizes the thermal behav-

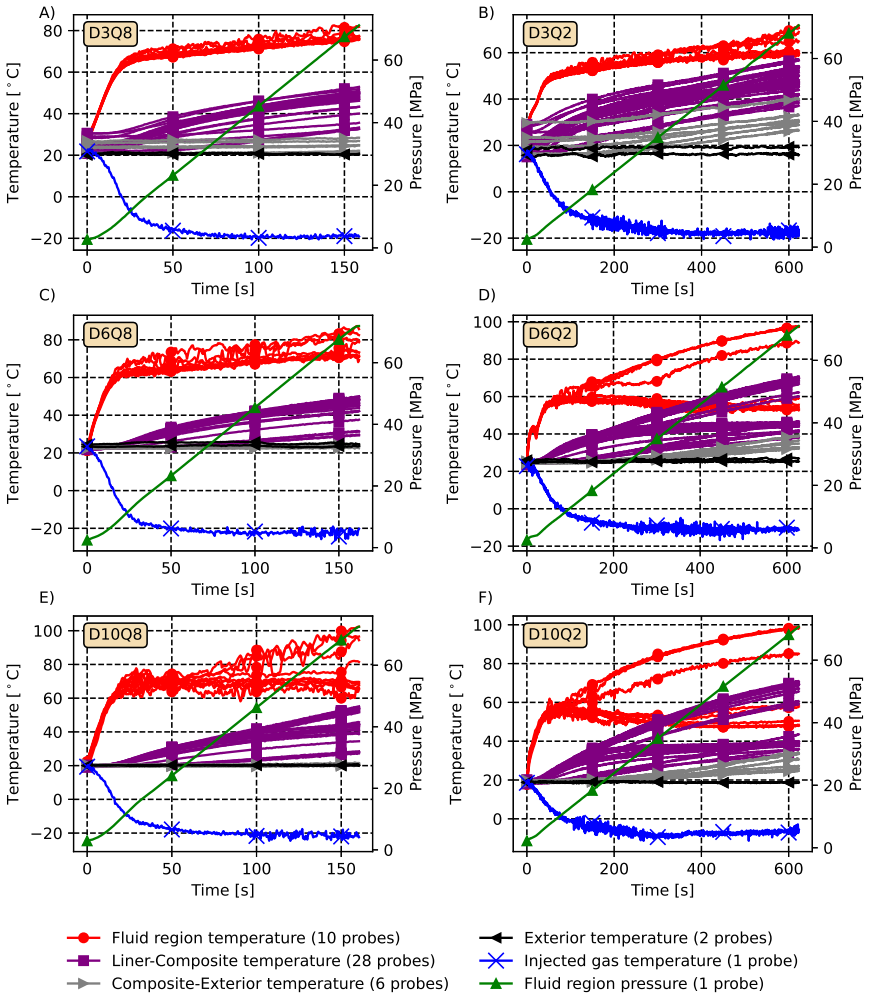

Figure 2: Experimental measurements from HyTransfer [13], for six cases: (A) D3Q8, (B) D3Q2, (C) D6Q8, (D) D6Q2, (E) D10Q8, (F) D10Q2. The number of temperature probes used in the different tank regions is added in brackets in the legend. The temperatures are indicated on the left axis and the pressure is indicated on the right axis

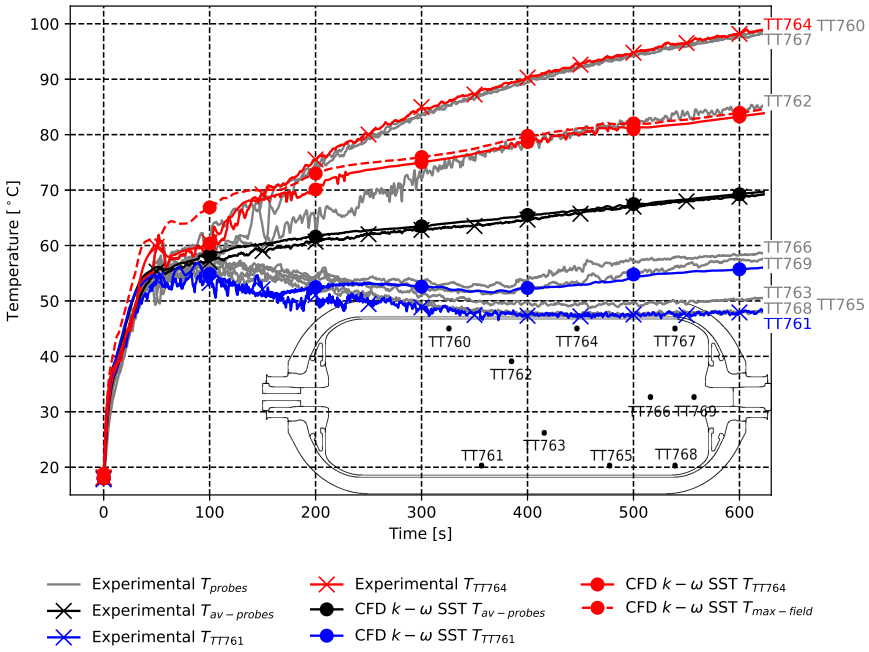

Figure 3: Scenario D10Q2. Comparison between the experimental measurements and CFD results using the $k-\omega$ SST model, concerning the averaged and local temperature values. The averaged temperature $T_{av-probes}$ is the arithmetic average of the 10 probe temperatures located in the fluid region. The maximum temperature value issued from the CFD thermal field is represented by a red dashed line.

ior in the tank, for the D10Q2 case, i.e. the most heterogeneous case. The averaged temperature in the tank (black) is plotted together with values from temperature probes (grey). The temperatures of the probes TT764 and TT761 exhibit the maximum and minimum values among probe data (red and blue, respectively). The average CFD temperature matches the experimental data ($T_{exp} - T_{CFD} = -0.12\ ^{\circ}C$). At probe TT764, CFD temperature is lower than the experimental one ($T_{exp} - T_{CFD} = 15.05\ ^{\circ}C$). At probe TT761, CFD temperature is higher than the experimental one ($T_{exp} - T_{CFD} = -8.01\ ^{\circ}C$). The maximum temperature in the CFD thermal field (red dashed line) is close to the CFD value at probe TT764.

The turbulence modeling approach could explain the deviation from the experimental data. The $k - \omega$ SST turbulence model tends to over-predict turbulent kinetic energy, leading to high values of the turbulent viscosity [18]. As the viscosity plays an important role in the thermal diffusion process, the $k - \omega$ SST turbulence model is suspected to over-predict thermal diffusion and thus to underestimate the thermal gradient magnitude.

The objective of this paper is to clarify the role of turbulence modeling in the thermal stratification process and to suggest a more accurate turbulence model for tank filling simulations.

Models based on Unsteady Reynolds-Averaged Navier–Stokes (URANS) approach are considered due to their reduced computational costs. To limit the turbulence level in areas where the flow may still be laminar, advanced turbulence models are considered.

A CFD case with no turbulence model is considered with the same mesh as in the previous D10Q2 simulation [14]. This case would work as a Direct Numerical Simulation (DNS) if the mesh and time step were fine enough. That is why this numerical experiment is called the coarse-DNS (cDNS) case. It aims at investigating the effect of turbulence modeling in the URANS equations, on the thermal field.

2. Physical system and modeling approach

2.1. Description of the physical system

Filling of a hydrogen tank consists in injecting pressurized gaseous hydrogen inside a closed vessel. In the tank, the pressure is rising due to the increase of mass and the temperature is rising due to the compression effect. Figure 1 presents a schematic of the tank geometrical configuration. The tank has a circular symmetry around its main axis, the x-axis. The gas is injected axially along the x-axis. The tank is placed horizontally and the gravity ($\mathbf{g}$) is pointing along the y-axis.

The solid regions of the tank are: (i) a composite wrap which supports the mechanical load of the gas pressure, (ii) a plastic liner which limits the molecular diffusion of hydrogen across the wall, (iii) metallic bosses, (iv) plugs at each tank extremities and (v) a metallic injection pipe.

The fluid region inside the tank can be defined by the remaining volume enclosed by the solid regions.

An ambient temperature and atmospheric pressure are in contact with the exterior tank walls.

Data from experimental measurements provided during the HyTransfer project [13] are used to initialize the simulations. During the experimental measurements, in the fluid region, the temperature was measured from 10 probes located as presented in figure 1. The inlet temperature is issued from a temperature probe located 10 cm upstream from the pipe inlet. Figure 2, adapted from [13], shows plots of all probe measurements in the tank for the different filling scenarios examined with the type IV 37 L tank.

2.2. Modeling approach

The simulations consists in a coupled CFD simulation in the fluid region and heat transfer simulation in solid regions, called Conjugate Heat Transfer (CHT) method [19].

The energy balance equation is solved in solid regions to simulate the thermal diffusion across tank walls. The set-up is the same as in a previous study on this topic [14].

The governing equations in the fluid region are the mass, momentum and energy balance equations.

The Reynolds number evaluated with the plug aperture diameter (10 mm) evolves from 45 000 to 15 000 during the filling. For these Reynolds numbers, the flow is turbulent in the injection area [20]. The turbulence is modeled using the URANS approach with the Boussinesq eddy-viscosity assumption [21].

For the velocity, a no-slip condition is applied on walls. As input, a mass flowrate is applied uniformly on the inlet with time-dependent values deduced from the experimental pressure ramp (see 2 (green line)). The temperature and heat flux are set to ensure continuity between the different regions.

Considering the present ranges of pressure and temperature, the hydrogen cannot be considered as an ideal gas [5]. Real gas data from the National Institute of Standards and Technology (NIST) [22] are used to determine the thermodynamics.

2.3. Turbulence modeling

In the URANS equation system [23], turbulence effects are taken into account via the Reynolds stress tensor τ_{ij} $[kg/m/s^2]$, which contributes to the total viscosity tensor. Using the Boussinesq eddy-viscosity assumption

$$\tau_{ij} = 2\mu_t S_{ij} - \frac{2}{3}\rho k \delta_{ij} \ , \tag{1}$$

the Reynolds stress tensor is linked to the turbulent viscosity μ_t $[kg/m/s]$, the turbulent kinetic energy k $[m^2/s^2]$, the Kronecker delta δ_{ij} [1] and the density ρ $[kg/m^3]$. The mean rate of strain tensor S_{ij} $[1/s]$ is

$$S_{ij} = \frac{1}{2}\left(\frac{\partial U_i}{\partial x_j} + \frac{\partial U_j}{\partial x_i}\right) \ , \tag{2}$$

where U $[m/s]$ is the Reynolds-Averaged velocity field. Turbulence models are designed to model τ_{ij} via μ_t $[kg/m/s]$. However, μ_t $[kg/m/s]$ also plays an important role in thermal diffusion. In the energy equation, the effective thermal conductivity λ_{eff} $[W/m/K]$ is defined as

$$\lambda_{eff} = \lambda + \lambda_t \ , \tag{3}$$

where λ is the thermal conductivity and λ_t is the turbulent thermal conductivity,

$$\lambda_t = \frac{c_p \mu_t}{Pr_t}, \tag{4}$$

where $Pr_t = 0.85$ is the turbulent Prandtl number and c_p $[J/kg/K]$ is the specific heat capacity. The effective thermal diffusivity is directly linked to the effective thermal conductivity:

$$\alpha_{eff} = \frac{\lambda_{eff}}{\rho c_p} \ . \tag{5}$$

The choice of the turbulence model is a key element for temperature prediction since it impacts the prediction of the turbulent viscosity and therefore the prediction of the effective thermal diffusivity.

A previous study [24] pointed out that the $k-\epsilon$ Realizable turbulence model is the most suitable for CFD simulation of hydrogen tank filling. The comparison test was performed for an axisymmetric case where gravity was not taken into account. The benchmark was based on the averaged temperature only. The influence of the different models on temperature distribution is unknown. This model was recently used to investigate the temperature distribution during the filling stage of a hydrogen tank [25, 26, 27]. The model captures correctly the round jet physics [28] which is an important part of the fluid dynamics in the tank. However, the thermal boundary layer at wall must be modeled by a wall function, which is problematic for precise heat transfer predictions [29].

Therefore, to improve the capture the thermal layer instead of modeled it with wall functions, the mesh at walls is refined and the $k-\omega$ SST turbulence model [17, 29] is selected. In previous studies [16, 14], this turbulence model was able to capture the averaged value of the temperature and the onset of stratification while underestimating thermal gradient amplitudes. The model involves two equations to predict the eddy-viscosity: one is based on the conservation of the turbulent kinetic energy k $[m^2/s^2]$ and the other one is based on the conservation of the specific rate of dissipation of the turbulent kinetic energy ω $[1/s]$.

The idea behind the $k-\omega$ SST turbulence model is to merge two other two-equations eddy-viscosity models, the $k-\omega$ and $k-\varepsilon$ models. An advantage of the $k-\omega$ model is to be applicable until the viscous layer. Its major downside is its sensitivity to the freestream condition [30], which can lead to less accurate predictions than the $k-\varepsilon$ model. Therefore, the $k-\omega$ SST turbulence model was designed to switch between the $k-\omega$ model close to walls and the $k-\varepsilon$ model in other regions. This model is intensively used in the industry [31].

A limitation of the $k-\omega$ SST model is the over-predicted turbulence kinetic energy in stagnation regions [18]. This becomes problematic when the cooled jet coming from the injected gas is deviated towards the lower part of the tank and the upper part of the tank becomes a stagnation area. Increasing the turbulent kinetic energy in this area would, from a thermal perspective, increase temperature diffusion and limit gradient amplitudes, which is consistent with the observations reported in the previous study [14]. Therefore, advanced turbulence models which limit the production of turbulent kinetic energy, and consequently turbulent viscosity, are expected to improve gradient predictions.

The $\gamma - Re_\theta$ model [32, 33] is a 4-equation model designed to capture the laminar-turbulent transition phenomenon. It is derived from the $k-\omega$ SST model and includes two additional equations for two additional variables: the intermittency γ and the momentum thickness Reynolds number Re_θ. It was used by the Joint Research Centre (JRC) of the European Commission [34, 35] to study the thermal distribution during hydrogen tank filling. It was able to detect the onset of stratification but underestimated the thermal amplitude, compared to the experimental measurements [34].

In a preliminary phase of the present study, several tests have been carried out using the $\gamma - Re_\theta$ model with OpenFOAM [36]. No substantial difference with the $k-\omega$ SST model has been noted and the investigation of the $\gamma - Re_\theta$ model was stopped.

The Scale Adaptive Simulation (SAS) concept was applied to the $k-\omega$ SST model [37] to avoid the over-prediction of eddy-viscosity. The SAS concept consists in comparing the turbulent length-scale L issued from the $k-\omega$ SST model to the von Kármán length scale $L_{\nu K}$, a three-dimensional generalization of the boundary layer thickness. Depending on the ratio $\frac{L}{L_{\nu K}}$, a source term Q_{SAS} is added in the balance equation of ω, correcting the production of ω, and therefore impacting the turbulent viscosity μ_t.

The model is available in OpenFOAM [38] and supplementary details can be found in [17, 37, 39]. The corrected value of turbulent viscosity μ_t in stagnation areas is expected to improve the prediction of temperature gradients.

In addition, to investigate the influence of the turbulent viscosity on the temperature field, a numerical experiment with no turbulence model is performed: the cDNS. In this case, the flow is considered to be fully resolved, i.e. the small scale structures of turbulence are filtered. This approach will therefore tend to minimize thermal diffusion and thus maximize temperature gradients. The equation system is the same as for DNS studies, although the mesh is not fine enough to capture the smallest scales, as theorized in the Kolmogorov theory [40]. For example, in the injection area, the smallest scale η $[m]$, can be linked to the Reynolds number $Re = \frac{u_{inj} D}{\nu}$ by the relationship $\eta \sim DRe^{-3/4}$, with the injection velocity u_{inj} $[m/s]$, the injection diameter D $[m]$ and the kinematic viscosity ν $[m^2/s]$. For the D10Q2 case, $Re \approx 1.5 \times 10^4$ at minimum, consequently this scale is at maximum $\eta = 7.3 \times 10^{-6}$ m. The smallest cell size is 4.9×10^{-5} m. The DNS conditions are not satisfied but the simulation may still give insights into the impact of turbulence modeling.

To save computational resources, the different simulations have been initialized at 180 s based on the $k-\omega$ SST results; this corresponds to the beginning of the thermal stratification.

3. Numerical Method

The OpenFOAM solver chtMultiRegionFoam [41] is used to perform the CHT simulations. In the fluid region, the solver uses the Pressure Implicit with Splitting of Operators (PISO) algorithm [42, 43]. A variable time step is used to maintain the Courant–Friedrichs–Lewy number (CFL) lower than 1 during the simulations.

A symmetry assumption is used to reduce CFD cost. Only half of the tank, cut through the (x,y) plane, is considered. The mesh is issued from the heterogeneous case described in the previous study [14]. It is composed of 651 482 cells in the fluid region and 449 126 cells in the solid regions, using hexahedral dominant meshes. In the fluid region, the minimal cell volume (1.17×10^{-13} m^3) is located in the injection area where the velocities are the highest and the maximal cell volume (2.6×10^{-7} m^3) is located in the main bulk. A $y^+ < 1$ numerical criterion on walls is maintained to avoid wall functions. The mesh is issued and was validated in a previous study [14].

4. Results

4.1. Comparison of thermal gradient predictions

Figure 4 shows a comparison of the CFD results with the experimental measurements. Averaged temperatures are calculated using an arithmetic average from local temperature probes. Concerning the averaged gas temperature, for all the CFD approaches, it matchs the experimental averaged gas temperature. Considering the maximum temperature, probe TT764, the $k-\omega$ SST case underestimates the temperature while the cDNS case overestimates it. The $k-\omega$ SST SAS case results are in-between, in better agreement with the experimental data than the other CFD approaches, even though slightly lower.

On the TT761 probe, the $k-\omega$ SST model overestimates the temperature while the cDNS case underestimates it. The $k-\omega$ SST SAS case is slightly higher than the experimental value.

The values of the averaged and probe temperature deviations ($T_{exp}-T_{CFD}$) at the final time (630 s) for the different CFD approaches are presented in table 2.

A detailed monitoring of each probe is presented in figure 5. It can be noted that the $k-\omega$ SST SAS case is closer to the experimental data on the higher and lower probes than on the central probes (TT762, TT766, TT769).

The $k-\omega$ SST SAS case shows better prediction of the thermal gradients (i.e. closer to the experimental data) than the $k-\omega$ SST and the cDNS cases.

$T_{exp} - T_{CFD}$ [°C]\CFD approaches	$k-\omega$ SST	$k-\omega$ SST SAS	cDNS
av(T) t_f [°C]	-0.12	0.11	-0.73
TT764 t_f [°C]	15.05	2.17	-4.82
TT761 t_f [°C]	-8.01	-1.79	5.66

Table 2: Temperature deviations between the experimental data and CFD simulation results at the end of the filling, for each CFD approach.

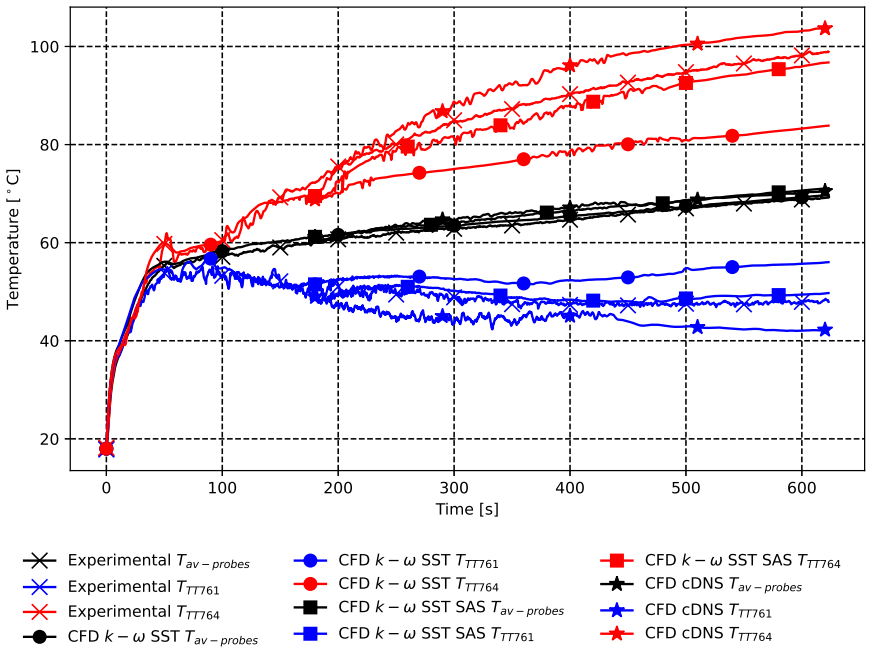

Figure 4: Scenario D10Q2. Comparaison between the experimental measurements and CFD results concerning the averaged and local temperature values, for each CFD approach. The results of the $k-\omega$ SST model simulation are issued from [14].

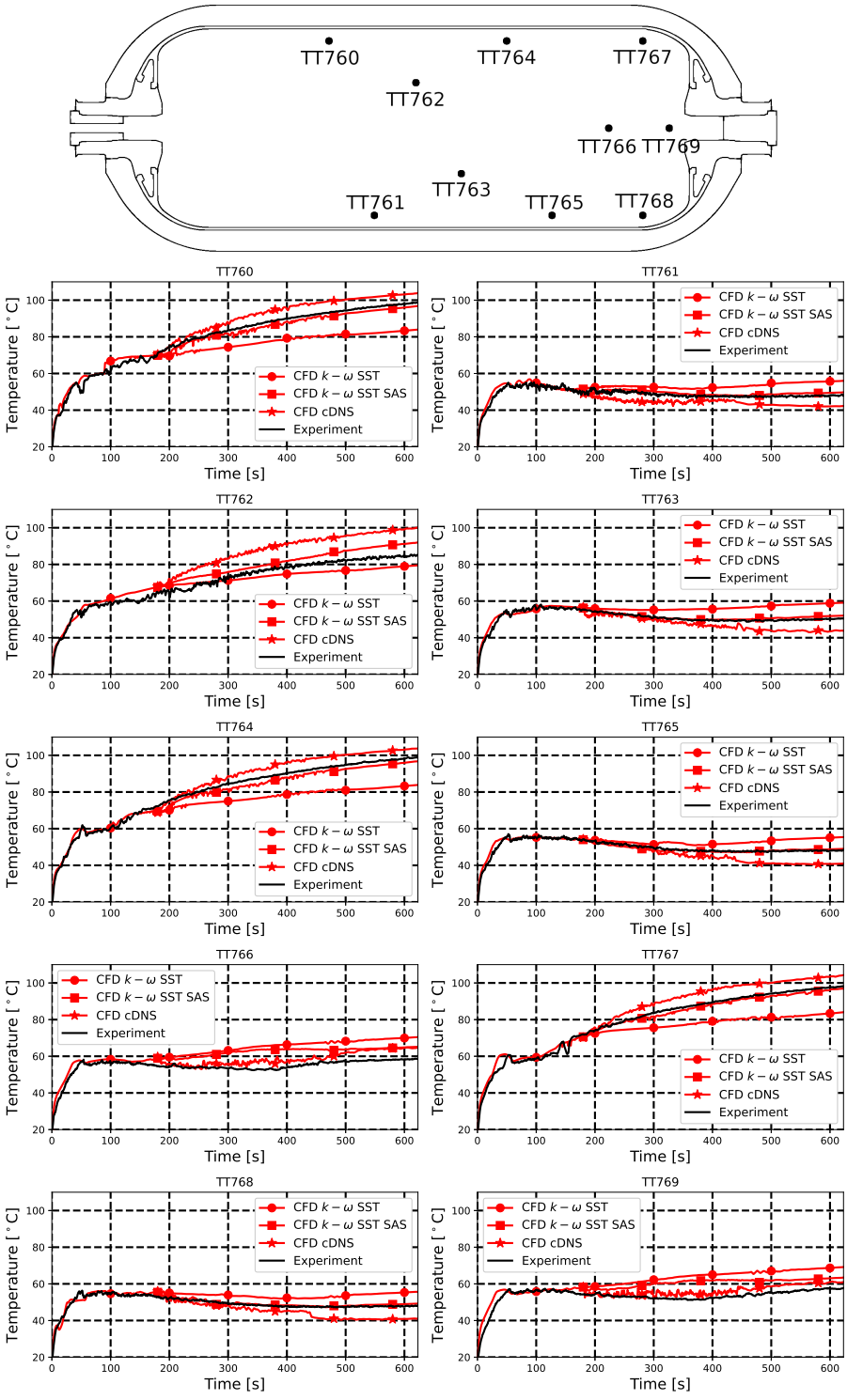

Figure 5: Scenario D10Q2. Comparison between the local temperatures issued from the simulations and the experiment. Probe locations are indicated at the top of the figure.

4.2. Field comparison

Figure 6 presents, for scenario D10Q2 at three instants (200 s, 400 s, 600 s), the temperature fields simulated by the $k-\omega$ SST (upper view) and $k-\omega$ SST SAS (lower view) turbulence models. Likewise, figure 7 depicts the effective thermal diffusivity. In figures 6 and 7, the fields are located in the symmetry plane.

The source term Q_{SAS}, added to the ω balance equation in the $k-\omega$ SST SAS model, limits the level of turbulent viscosity. The effective thermal diffusivity behaves like the turbulent viscosity (expression (5)). Figure 7 shows that the level of effective thermal diffusivity is reduced when the $k-\omega$ SST SAS model is used. In the stagnation area where there is no mixing, the lower effective thermal diffusivity strongly influences the temperature field. Figure 6 shows that, for each time instant, the averaged temperature (given above the thermal field) is similar for the two turbulence models, while the maximum temperature (also reported above the thermal field) is significantly different. For example at 600 s, the difference of maximum temperature between the $k-\omega$ SST SAS and $k-\omega$ SST turbulence models reaches approximately 13 $°C$.

A complementary video of scenario D10Q2 using the $k-\omega$ SST SAS model is available in the **Supplemental Data**. It presents the thermal field in the upper view and the velocity field in the lower view.

5. Application to other filling scenarios

The comparison reported in section 4 shows that the $k-\omega$ SST SAS turbulence model substantially improves the thermal gradient prediction for scenario D10Q2. Two other filling scenarios are selected to confirm the accuracy of this approach, scenarios D6Q2 and D6Q8.

For both scenarios, a mesh composed of 704 209 cells in the fluid region is employed. The processing time depends on the solver algorithm and the inlet velocity. It has been found that the PISO solver is computationally more efficient for velocities below $10-20$ m/s while the PIMPLE algorithm [44] is faster for higher velocities, using a $CFL > 1$. Consequently, a PIMPLE-PISO switch has been performed at 100 s for scenario D6Q2 and at 80 s for scenario D6Q8.

5.1. Scenario D6Q2

Like scenario D10Q2, scenario D6Q2 leads to a large difference between the averaged and maximum gas temperatures issued from the probes (figure 2,D), $T_{max}-T_{av} = 30.03$ $°C$ and $T_{max}-T_{av} = 26.76$ $°C$, respectively. Unlike scenario D10Q2, scenario D6Q2 involves an injection pipe, which is usually present during tank filling in real conditions.

Figure 8 compares the average and local probe temperatures issued from the experimental measurements with the CFD results. For scenario D6Q2, measurements from the probes TT760, TT764 and TT767 tend to converge during the filling. The probe TT760 temperature rises at 90 s, then the probe

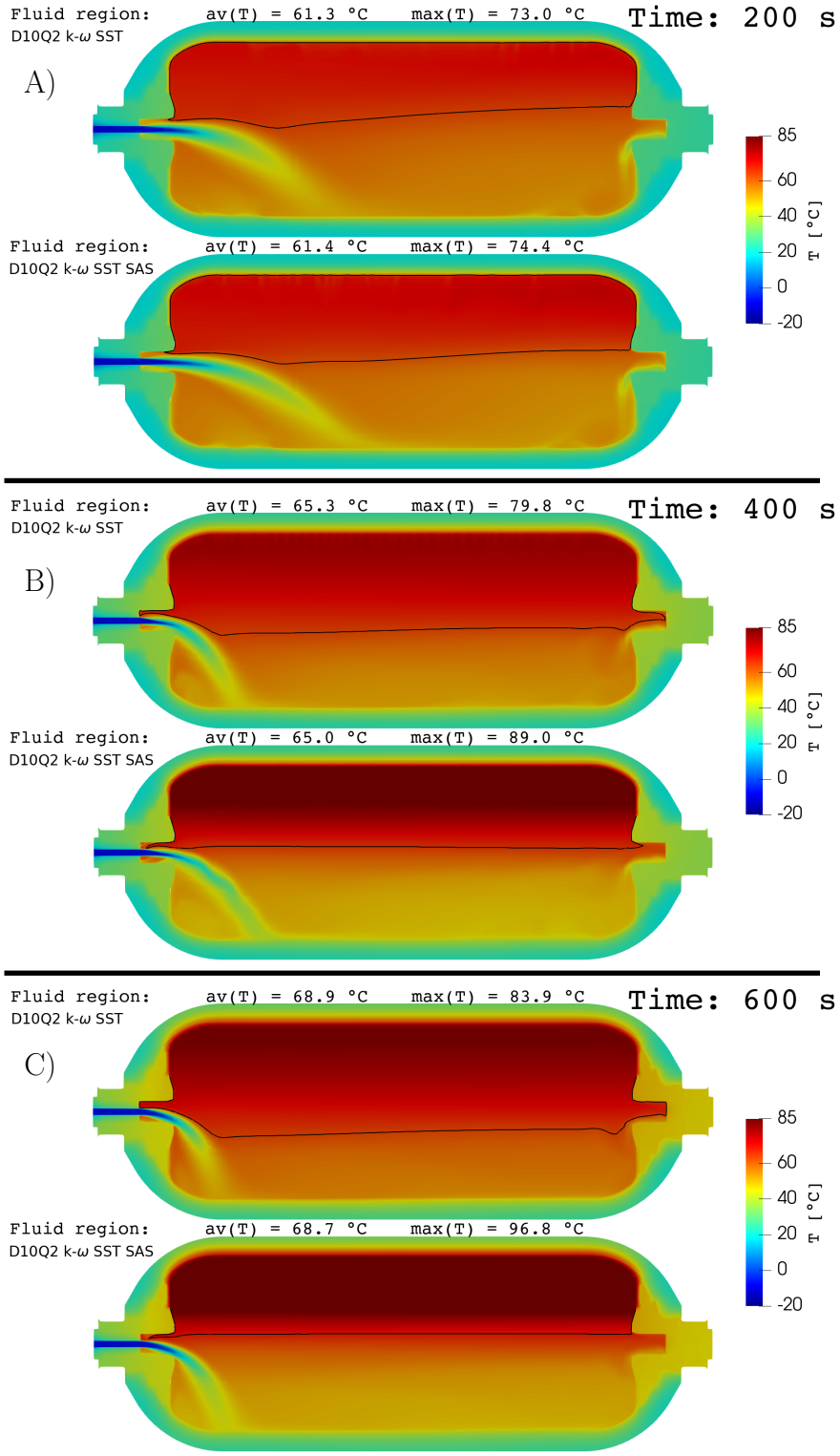

Figure 6: Scenario D10Q2. Comparison of the temperature fields predicted by the $k-\omega$ SST (upper views) and $k-\omega$ SST SAS (lower views) turbulence models, at three time instants: (A) 200 s, (B) 400 s and (C) 600 s. The black line corresponds to the isoline of averaged temperature.

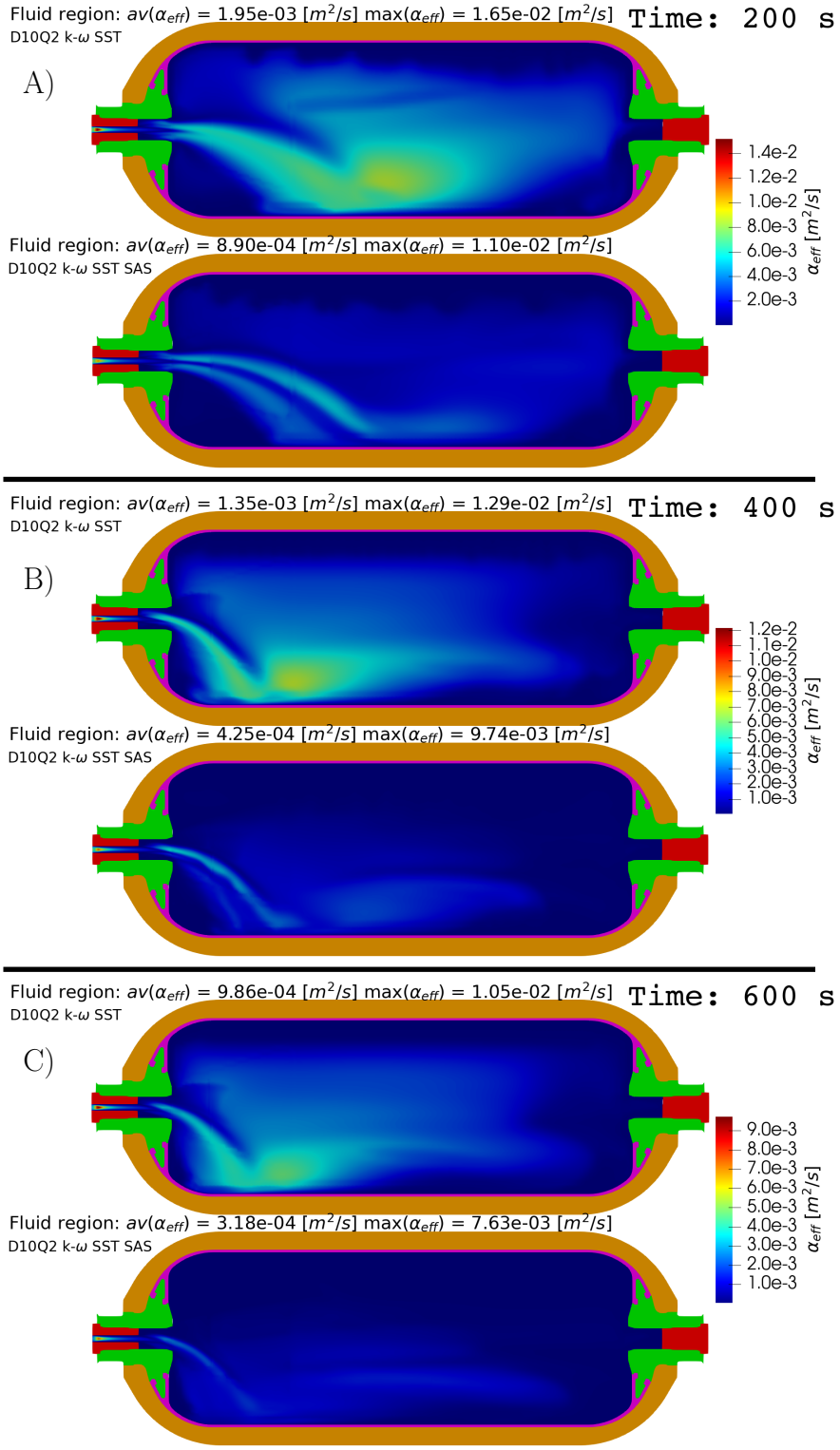

Figure 7: Scenario D10Q2. Comparison of the effective thermal diffusivity fields predicted by the $k-\omega$ SST (upper views) and $k-\omega$ SST SAS (lower views) turbulence models, at three time instants: (A) 200 s, (B) 400 s and (C) 600 s.

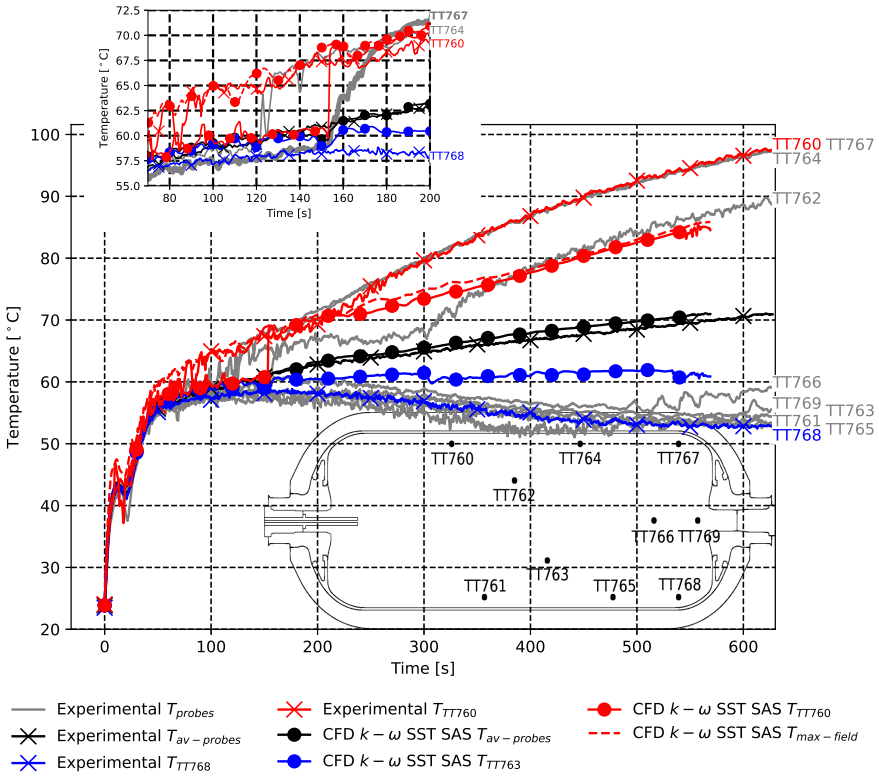

Figure 8: Scenario D6Q2. Comparison between the averaged and local temperature values issued from the experimental measurements and the CFD results using the $k-\omega$ SST SAS turbulence model. The maximum temperature value issued from the CFD thermal field is represented by a red dashed line. The upper view is a zoomed view in the time interval [70 s 200 s], to see the delay of probe TT760 temperature between the CFD and experimental results.

TT764 temperature at 130 s and finally the probe TT767 temperature at 180 s. At the final time, the temperatures measured by probes TT760, TT764 and TT767 are very close. The CFD results predict a similar phenomenon, i.e. a local increase of temperature (a hot spot) occurs near the injection region where the gas is not cooled by the injected gas. Once the buoyancy forces dominate the jet momentum forces, the jet is deflected and the hot spot is convected along the upper part, crossing successively probes T760, TT764 and TT767. Figure 9 shows that the hot spot is close to the injector region at $t = 150$ s. At $t = 200$ s, the hot spot has already crossed probes TT760 and TT764 but not probe TT767. At $t = 450$ s, the hot spot has reached the rear region of the tank. The CFD predicts this phenomenon with a delay compared to the experimental measurements. In figure 8, the temperature raise for probe TT760 occurs at 150 s in the CFD results versus 90 s in the experiment.

After 150 s, the maximum gas temperature issued from the CFD results (red dashed line) is similar to the temperature from probe TT760. This suggests that probe TT760 is correctly located to measure the maximum temperature in the tank at the end of the filling.

The CFD simulation predicts a lower vertical thermal gradient than that measured experimentally. At time $t = 568.9$ s, the difference of temperature for probe TT760 between the experimental measurements and the CFD results is $T_{exp} - T_{CFD} = 10.1$ $°C$. The difference for probe TT768 is $T_{exp} - T_{CFD} = -8.02$ $°C$.

The difference between the experimental measurements and the CFD results are larger than for the D10Q2 scenario. No results issued from the $k - \omega$ SST model are available and the impact of the SAS approach cannot be estimated for the D6Q2 scenario.

These discrepancies could be explained by the presence of the experimental measurement device in the gas region. A thermocouple tree (figure 10)has been inserted in the rear region of the tank (region opposite to the injector region). Considering the D6Q2 configuration, with an injection pipe, the injection outlet is closer to the thermocouple tree extremity. This results in a potential interaction between the jet and the measurement device, leading possibly to less thermal mixing and larger thermal gradients. Moreover, the jet is deflected earlier in the D10Q2 scenario. Figures 6 and 9 show that in this scenario, at $t = 200$ s, the jet is more deflected than in the D6Q2 scenario at $t = 450$ s, reducing the potential influence of the measurement device in the D10Q2 scenario. The influence of the experimental measurement device on the actual thermal field remains to be clarified.

5.2. Scenario D6Q8

Scenario D6Q8 leads to a limited gradient, with a maximum of 11.28 $°C$ between the averaged and maximum gas temperatures issued from the probes (figure 2,C)). It represents an interesting case to test the $k - \omega$ SST SAS turbulence model in a scenario involving an important thermal mixing by the inner jet.

Figure 11 compares the average and local probe temperatures issued from the experimental measurements and the CFD simulation. The minimum temperature is not observed at the lowest probes (TT761,TT765,TT768), but at the TT763 probe. This can be explained as follows: due to the gravity, the cold jet is deflected and hits the TT763 probe, which is closer to the injector outlet than the TT765 probe. The averaged and local temperatures predicted by the CFD simulation are close to the experimental measurements.

The jet oscillates in the tank. By oscillating up and down, it successively cools down the upper part and the lower part of the tank. The temperatures from probes TT763 and TT760 oscillate in phase opposition (figure 11). When the jet stops oscillating (close to 70 s), the same phenomenon as for scenario D6Q2 occurs: with the deflection of the jet, a hot spot is convected from the injector region to the tank rear region, and a vertical thermal gradient develops.

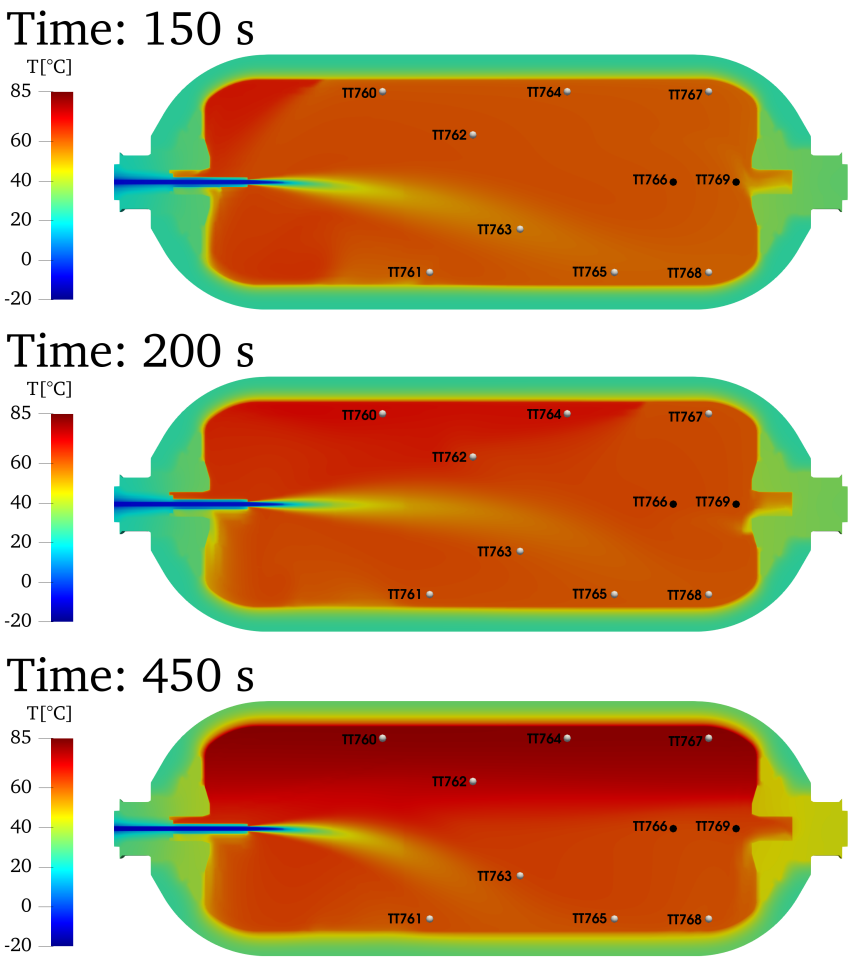

Figure 9: Scenario D6Q2. CFD simulation using the $k-\omega$ SST SAS turbulence model. The temperature field in the (x,y) plane is reported at time $t = 150\ s$, $t = 200\ s$ and $t = 450\ s$. The convection of the hot spot is visible between $t = 150\ s$ and $t = 200\ s$.

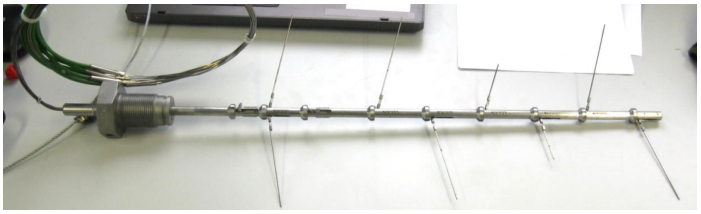

Figure 10: Thermocouple tree photograph reproduced from the report concerning the experimental tests of the HyTransfer project [13].

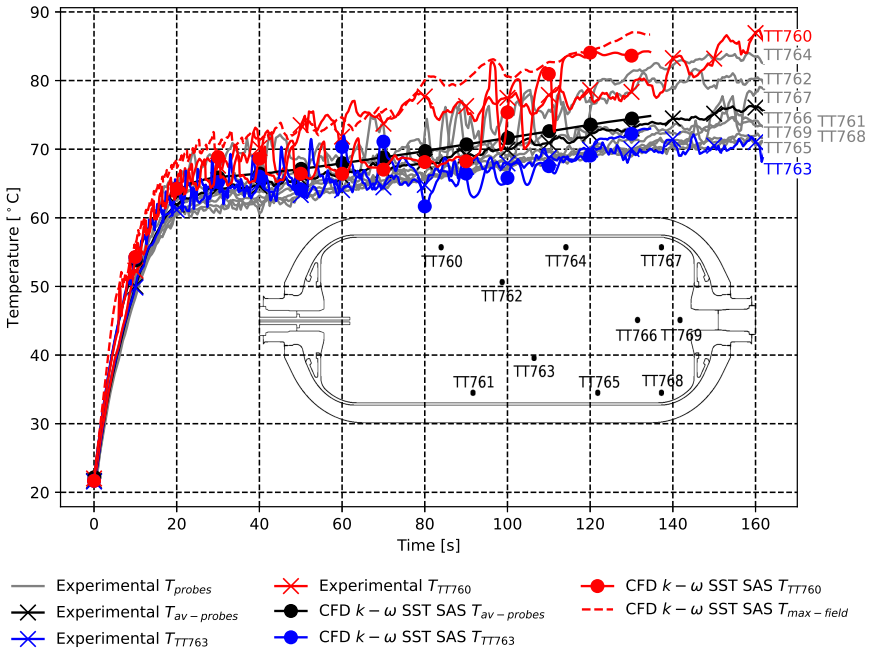

Figure 11: Scenario D6Q8. Comparison between the averaged and local temperature values issued from the experimental measurements and the CFD results using the $k-\omega$ SST SAS turbulence model. The maximum temperature value issued from the CFD thermal field is represented by a red dashed line.

Complementary videos of scenarios D6Q2 and D6Q8 using the $k-\omega$ SST SAS model are available in the **Supplemental Data**.

6. Conclusion

The objective of this work was to improve the CFD prediction of thermal gradients during the filling stage of a hydrogen tank. Previous studies [16, 34, 14] had shown that the URANS approach, associated with the $k-\omega$ SST turbulence model, tends to underestimate thermal gradients. Here, the impact of turbulence modeling on thermal gradient prediction was investigated on an experimental case, issued from the HyTransfer project [12] and leading to large thermal gradients. The underprediction of the thermal gradient magnitude by the $k-\omega$ SST model was attributed to an overestimation of the eddy-viscosity, which plays a key role in thermal diffusion. An advanced turbulence model, the $k-\omega$ SST SAS model, was used to balance the eddy-viscosity production, and it was shown to substantially improve the prediction for this filling scenario.

The accuracy of the $k-\omega$ SST SAS model was assessed on a second filling scenario leading to large thermal gradients. The CFD results underestimate the maximum gas temperature by 10.1 $°C$, compared to the experimental measurements. This difference could be attributed to the measurement device present in the tank during the experiments, which may potentially interact with the jet. The impact of the measurement device on thermal mixing needs to be clarified.

The $k-\omega$ SST SAS turbulence model leads to accurate predictions for a third scenario with limited thermal gradients. It requires similar computational resources compared to the $k-\omega$ SST turbulence model. Consequently, the present study suggests to use the $k-\omega$ SST SAS turbulence model for CFD simulation of tank filling.

Acknowledgment

This study was carried of as part of a PhD work funded by Air Liquide Innovation Campus Paris and the National Association of Recherche and Technology (ANRT). It was performed using HPC resources from CALMIP (grants 2019, 2020, 2021 and 2022 p19025).

References

[1] UNFCCC, Conference of the parties serving as the meeting of the parties to the paris agreement (2021).
URL `https://unfccc.int/sites/default/files/resource/cma2021_L16_adv.pdf`

[2] Hydrogen for net-zero : A critical cost-competitive energy vector (2021).
URL `https://hydrogencouncil.com/wp-content/uploads/2021/11/Hydrogen-for-Net-Zero.pdf`

[3] Q. Nouvelot, P. Karzel, N. Hart, E. Vyazmina, V. Mattelaer, C. D. Sinding, A. Ruiz, Performance metrics for refuelling protocols for heavy duty hydrogen vehicules, fCH-04-2-2019:Refuelling Protocols for Medium and Heavy-Duty Vehicules (2020).
URL https://prhyde-cdn.s3-accelerate.amazonaws.com/wp-content/uploads/2020/10/14133040/PRHYDE_Deliverable-D2-1_final.pdf

[4] F. C. S. Committee, Fueling protocols for light duty gaseous hydrogen surface vehicles (dec 2016). doi:https://doi.org/10.4271/J2601_201612.
URL https://doi.org/10.4271/J2601_201612

[5] D. Melideo, D. Baraldi, M. C. Galassi, R. Ortiz Cebolla, B. Acosta Iborra, P. Moretto, CFD model performance benchmark of fast filling simulations of hydrogen tanks with pre-cooling, International Journal of Hydrogen Energy 39 (9) (2014) 4389–4395. doi:https://doi.org/10.1016/j.ijhydene.2013.12.196.
URL https://www.sciencedirect.com/science/article/pii/S0360319913031881

[6] D. Melideo, D. Baraldi, CFD analysis of fast filling strategies for hydrogen tanks and their effects on key-parameters, International Journal of Hydrogen Energy 40 (1) (2015) 735–745. doi:https://doi.org/10.1016/j.ijhydene.2014.10.138.
URL https://www.sciencedirect.com/science/article/pii/S0360319914030146

[7] C. Dicken, W. Mérida, Measured effects of filling time and initial mass on the temperature distribution within a hydrogen cylinder during refuelling, Journal of Power Sources 165 (1) (2007) 324–336. doi:https://doi.org/10.1016/j.jpowsour.2006.11.077.
URL https://www.sciencedirect.com/science/article/pii/S0378775306024244

[8] G. Wang, J. Zhou, S. Hu, S. Dong, P. Wei, Investigations of filling mass with the dependence of heat transfer during fast filling of hydrogen cylinders, International Journal of Hydrogen Energy 39 (9) (2014) 4380–4388. doi:https://doi.org/10.1016/j.ijhydene.2013.12.189.
URL https://www.sciencedirect.com/science/article/pii/S0360319913031819

[9] T. Terada, H. Yoshimura, Y. Tamura, H. Mitsuishi, S. Watanabe, Thermal behavior in hydrogen storage tank for fcv on fast filling (2nd report) (2008). doi:10.4271/2008-01-0463.
URL https://www.sae.org/content/2008-01-0463/

[10] T. Bourgeois, T. Brachmann, F. Barth, F. Ammouri, D. Baraldi, D. Melideo, B. Acosta-Iborra, D. Zaepffel, D. Saury, D. Lemonnier, Optimization of hydrogen vehicle refuelling requirements,

International Journal of Hydrogen Energy 42 (19) (2017) 13789–13809, special Issue on The 21st World Hydrogen Energy Conference (WHEC 2016), 13-16 June 2016, Zaragoza, Spain. doi:https://doi.org/10.1016/j.ijhydene.2017.01.165.
URL https://www.sciencedirect.com/science/article/pii/S0360319917303312

[11] N. de Miguel, B. Acosta, P. Moretto, R. Ortiz Cebolla, Influence of the gas injector configuration on the temperature evolution during refueling of on-board hydrogen tanks, International Journal of Hydrogen Energy 41 (42) (2016) 19447–19454. doi:https://doi.org/10.1016/j.ijhydene.2016.07.008.
URL https://www.sciencedirect.com/science/article/pii/S0360319916307340

[12] E. i. European Commission, E. researchers, Hytransfer, FCH JU 2012-1-325277 (2013).
URL https://cordis.europa.eu/project/id/325277/reporting

[13] B. Ravinel, B. Acosta, N. De Migue, P. Moretto, O.-C. Rafael, J. Goran, v. d. L. Ulrich, D4.1 report on the experimental filling test campaign (2017).
URL https://s02291b7740b89df1.jimcontent.com/download/version/1493713659/module/11623534399/name/HyTransfer_Report%20on%20the%20experimental%20filling%20test%20campaign_public.pdf

[14] A computational fluid dynamic study of the filling of a gaseous hydrogen tank under two contrasted scenarios, International Journal of Hydrogen Energy 47 (55) (2022) 23278–23292. doi:https://doi.org/10.1016/j.ijhydene.2022.03.260.
URL https://www.sciencedirect.com/science/article/pii/S0360319922014100

[15] The OpenFOAM foundation (2022).
URL https://openfoam.org/

[16] D. Zaepffel, F. Mathey, B. Ravinel, T. Bourgeois, F. Ammouri, CFD analysis of the different flow regimes occurring during the filling of a hydrogen vehicle tank (2016).

[17] F. R. Menter, Two-equation eddy-viscosity turbulence models for engineering applications, AIAA Journal 32 (8) (1994) 1598–1605. doi:10.2514/3.12149.
URL https://arc.aiaa.org/doi/10.2514/3.12149

[18] F. R. Menter, A. R. Center., Improved two-equation k - [omega] turbulence models for aerodynamic flows [microform] / Florian R. Menter, National Aeronautics and Space Administration, Ames Research Center ; National

Technical Information Service, distributor Moffett Field, Calif. : [Springfield, Va, 1992.

[19] T. Perelman, On conjugated problems of heat transfer, International Journal of Heat and Mass Transfer 3 (4) (1961) 293–303. doi:https://doi.org/10.1016/0017-9310(61)90044-8.
URL https://www.sciencedirect.com/science/article/pii/0017931061900448

[20] B. Eckhardt, T. M. Schneider, B. Hof, J. Westerweel, Turbulence transition in pipe flow, Annual Review of Fluid Mechanics 39 (1) (2007) 447–468. doi:10.1146/annurev.fluid.39.050905.110308.
URL http://www.annualreviews.org/doi/10.1146/annurev.fluid.39.050905.110308

[21] F. G. Schmitt, About boussinesq's turbulent viscosity hypothesis: historical remarks and a direct evaluation of its validity, Comptes Rendus Mécanique 335 (9) (2007) 617–627, joseph Boussinesq, a Scientist of bygone days and present times. doi:https://doi.org/10.1016/j.crme.2007.08.004.
URL https://www.sciencedirect.com/science/article/pii/S1631072107001386

[22] E. Lemmon, M. Huber, M. McLinden, Nist standard reference database 23: reference fluid thermodynamic and transport properties-refprop, version 9.1 (2013-05-07 2013).
URL https://tsapps.nist.gov/publication/get_pdf.cfm?pub_id=912382

[23] R. Manceau, Industrial codes for CFD, lecture (Feb. 2021).
URL https://hal.inria.fr/hal-03207431

[24] A. Suryan, H. D. Kim, T. Setoguchi, Comparative study of turbulence models performance for refueling of compressed hydrogen tanks, International Journal of Hydrogen Energy 38 (22) (2013) 9562–9569. doi:10.1016/j.ijhydene.2012.07.055.
URL https://app.dimensions.ai/details/publication/pub.1025692856

[25] V. Ramasamy, E. Richardson, Thermal response of high-aspect-ratio hydrogen cylinders undergoing fast-filling, International Journal of Heat and Mass Transfer 160 (2020) 120179. doi:https://doi.org/10.1016/j.ijheatmasstransfer.2020.120179.
URL https://www.sciencedirect.com/science/article/pii/S001793102033115X

[26] H. Li, Z. Lyu, Y. Liu, M. Han, H. Li, The effects of infill on hydrogen tank temperature distribution during fast fill, International Journal of Hydrogen Energy 46 (17) (2021) 10396–10410. doi:https://doi.org/10.1016/j.ijhydene.2020.12.133.

URL https://www.sciencedirect.com/science/article/pii/S0360319920347479

[27] X. Wu, J. Liu, J. Shao, G. Deng, Fast filling strategy of type iii on-board hydrogen tank based on time-delayed method, International Journal of Hydrogen Energy 46 (57) (2021) 29288–29296. doi:https://doi.org/10.1016/j.ijhydene.2021.01.094.
URL https://www.sciencedirect.com/science/article/pii/S0360319921001865

[28] T.-H. Shih, W. W. Liou, A. Shabbir, Z. Yang, J. Zhu, A new k-epsilon eddy viscosity model for high reynolds number turbulent flows, Computers & Fluids 24 (3) (1995) 227–238. doi:https://doi.org/10.1016/0045-7930(94)00032-T.
URL https://www.sciencedirect.com/science/article/pii/004579309400032T

[29] F. Menter, T. Esch, Element of industrial heat transfer predictions (2001).

[30] F. R. Menter, Influence of freestream values on k-omega turbulence model predictions, AIAA Journal 30 (6) (1992) 1657–1659. arXiv:https://doi.org/10.2514/3.11115, doi:10.2514/3.11115.
URL https://doi.org/10.2514/3.11115

[31] F. Menter, M. Kuntz, R. Langtry, Ten years of industrial experience with the sst turbulence model, Heat and Mass Transfer 4 (01 2003).

[32] F. R. Menter, R. Langtry, S. Völker, Transition modelling for general purpose CFD codes 77 (1) 277–303. doi:10.1007/s10494-006-9047-1.
URL http://link.springer.com/10.1007/s10494-006-9047-1

[33] R. B. Langtry, F. R. Menter, Correlation-based transition modeling for unstructured parallelized computational fluid dynamics codes, AIAA Journal 47 (12) (2009) 2894–2906. doi:10.2514/1.42362.
URL https://arc.aiaa.org/doi/10.2514/1.42362

[34] D. Melideo, D. Baraldi, N. De Miguel Echevarria, B. Acosta Iborra, ICHS 2017: Effects of the injector direction on the temperature distribution during filling of hydrogen tanks, HySafe, 2017.
URL https://www.hysafe.info/ichs2017/

[35] D. Melideo, D. Baraldi, N. De Miguel Echevarria, B. Acosta Iborra, Effects of some key-parameters on the thermal stratification in hydrogen tanks during the filling process, International Journal of Hydrogen Energy 44 (26) (2019) 13569–13582. doi:10.1016/j.ijhydene.2019.03.187.
URL https://linkinghub.elsevier.com/retrieve/pii/S0360319919312169

[36] Langtry-menter k-omega shear stress transport (sst) (2021).
URL https://www.openfoam.com/documentation/guides/latest/doc/guide-turbulence-ras-k-omega-sst-lm.html

[37] F. Menter, Y. Egorov, A Scale Adaptive Simulation Model using Two-Equation Models. arXiv:https://arc.aiaa.org/doi/pdf/10.2514/6.2005-1095, doi:10.2514/6.2005-1095.
URL https://arc.aiaa.org/doi/abs/10.2514/6.2005-1095

[38] Scale-adaptive simulation based on the k-omega-sst (2021).
URL https://www.openfoam.com/documentation/guides/latest/api/classFoam_1_1RASModels_1_1kOmegaSSTSAS.html

[39] Y. Egorov, F. Menter, Development and application of sst-sas turbulence model in the desider project (2008).

[40] D. S.-K. Ting, Chapter 4 - turbulence scales, in: D. S.-K. Ting (Ed.), Basics of Engineering Turbulence, Academic Press, 2016, pp. 69–98. doi:https://doi.org/10.1016/B978-0-12-803970-0.00004-0.
URL https://www.sciencedirect.com/science/article/pii/B9780128039700000040

[41] ChtMultiRegionFoam (2021).
URL https://openfoamwiki.net/index.php/ChtMultiRegionFoam

[42] The PISO algorithm in OpenFOAM (2021).
URL http://openfoamwiki.net/index.php/OpenFOAM_guide/The_PISO_algorithm_in_OpenFOAM

[43] R. Issa, Solution of the implicitly discretised fluid flow equations by operator-splitting, Journal of Computational Physics 62 (1) (1986) 40–65. doi:https://doi.org/10.1016/0021-9991(86)90099-9.
URL https://www.sciencedirect.com/science/article/pii/0021999186900999

[44] The PIMPLE algorithm in OpenFOAM (2021).
URL https://openfoamwiki.net/index.php/OpenFOAM_guide/The_PIMPLE_algorithm_in_OpenFOAM